Kinetics and regulation of a Ca^{2+}-activated Cl^- conductance in mouse renal inner medullary collecting duct cells

S. H. Boese, O. Aziz, N. L. Simmons, and M. A. Gray

School of Cell and Molecular Biosciences, University Medical School, Newcastle Upon Tyne, NE2 4HH, United Kingdom

Boese, S. H., O. Aziz, N. L. Simmons, and M. A. Gray. Kinetics and regulation of a Ca^{2+}-activated Cl^- conductance in mouse renal inner medullary collecting duct cells. *Am J Physiol Renal Physiol* 286: F682–F692, 2004. First published December 16, 2003; 10.1152/ajprenal.00123.2003.—Using the whole cell patch-clamp technique, a Ca^{2+}-activated Cl^- conductance (CaCC) was transiently activated by extracellular ATP (100 μM) in primary cultures of mouse inner medullary collecting duct (IMCD) cells and in the mouse IMCD-K2 cell line. ATP also transiently increased intracellular Ca^{2+} concentration ($[Ca^{2+}]_i$) from ~100 nM to peak values of ~750 nM in mIMCD-K2 cells, with a time course similar to the ATP-induced activation and decay of the CaCC. Removal of extracellular Ca^{2+} had no major effect on the peak Cl^- conductance or the increase in $[Ca^{2+}]_i$ induced by ATP, suggesting that Ca^{2+} released from intracellular stores directly activates the CaCC. In mIMCD-K2 cells, a rectifying time- and voltage-dependent current was observed when $[Ca^{2+}]_i$ was fixed via the patch pipette to between 100 and 500 nM. Maximal activation occurred at ~1 μM $[Ca^{2+}]_i$, with currents losing any kinetics and displaying a linear current-voltage relationship. From Ca^{2+}-dose-response curves, an EC_{50} value of ~650 nM at −80 mV was obtained, suggesting that under physiological conditions the CaCC would be near fully activated by mucosal nucleotides. Noise analysis of whole cell currents in mIMCD-K2 cells suggests a single-channel conductance of 6–8 pS and a density of ~5,000 channels/cell. In conclusion, the CaCC in mouse IMCD cells is a low-conductance, nucleotide-sensitive Cl^- channel, whose activity is tightly coupled to changes in $[Ca^{2+}]_i$ over the normal physiological range.

renal collecting duct; calcium-activated chloride conductance; intracellular calcium

STUDIES USING PRIMARY CULTURES of rat inner medullary collecting duct (IMCD) cells (65), established cell lines derived from the IMCD (28, 29, 31, 32, 56), and most recently from fluid secretory studies from isolated native rat IMCD (61), have provided strong evidence that this renal segment is capable of net transepithelial Cl^- secretion, in addition to net Na^+ absorption (16). Through these two processes, the IMCD is ideally placed to determine final urinary salt composition through the regulatory action of natriuretic hormones and paracrines that act on this segment (16, 65). While the nature and regulation of Na^+ transport are clearly established in the IMCD (7, 55, 59, 64), less is known about the anion exit pathways mediating net transepithelial Cl^- secretion. Our previous patch-clamp studies identified two distinct apically located Cl^- conductances in the IMCD cell line mIMCD-K2 (3, 4, 33). This cell line was originally derived from the initial, outer portion of the inner medulla from a mouse transgenic for SV40 and was first characterized by Kizer et al. (31, 32). The

mIMCD-K2 cell line retains features typical of the IMCD, for instance, a mineralocorticoid-sensitive net Na^+ absorption blocked by amiloride and cAMP-stimulated electrogenic Cl^- secretion (31, 32). This cAMP-stimulated Cl^- secretion is mediated by apical expression of CFTR (3, 40, 56), which is well characterized in IMCD cells.

Recently, we have reported coexpression of a Ca^{2+}-activated Cl^- conductance (CaCC) together with CFTR in mIMCD-K2 cells (3, 4). During whole cell patch-clamp recordings, Ca^{2+}-mobilizing agonists led to the activation of a DIDS-sensitive Cl^- conductance with distinct biophysical properties to CFTR (3, 4). Although the Ca^{2+}-activated currents showed little kinetics after maximal stimulation, pronounced current relaxations could be observed when cytosolic Ca^{2+} was slowly increased (using prolonged ionomycin exposure under high intracellular Ca^{2+}-buffering conditions), suggesting that cytosolic Ca^{2+} controls the gating/kinetics of the channels (3).These properties of the CaCC in mIMCD-K2 cells are similar to the Ca^{2+}-activated conductances described in renal distal/collecting duct epithelial cells (1, 38), as well as to those in some typical secretory epithelia, (18, 30, 35), including the airways (54), suggesting that CaCCs in the IMCD are likely to have an important physiological role in Cl^- transport in this segment. However, precisely defining this role is problematic for a number of reasons. First, whether Ca^{2+}-activated Cl^- channels are present in native IMCD cells is not known. Second, we do not have sufficient information about the basic biophysical and regulatory properties of the underlying channels to establish whether they could contribute to net anion secretion and/or absorption in the IMCD under physiological conditions. Finally, as the molecular identity of the renal Ca^{2+}-activated ion channel is not firmly established, gene knockout or knockdown studies that could help provide definitive answers to the role of the CaCC in the IMCD cannot be performed. However, some recent progress has been made regarding the latter problem. Currently, there are two gene families that are potential molecular candidates for Ca^{2+}-activated Cl^- channels in mammalian cells. The CLCA family includes a group of 11 structurally related proteins that appear to be multifunctional, mediating cellular adhesion, tumor suppression, mucus production, as well as Cl^- transport (20). Of the 11 cloned family members, 6 of the isoforms have been shown to induce/confer a CaCC after functional expression in cell lines (COS-7, HEK-293T, NIH/3T3) and *Xenopus laevis* oocytes (bCLCA1, mCLCA1, mCLCA4, hCLCA1, hCLCA2, and pCLCA1). While the biophysical and pharmacological properties of the heterologously expressed CLCA proteins vary

Address for reprint requests and other correspondence: M. A. Gray, School of Cell and Molecular Bioscience, Univ. Medical School, Newcastle Upon Tyne, NE2 4HH, UK (E-mail: m.a.gray@ncl.ac.uk).

somewhat between isoforms (and even between expression systems; see Ref. 12), the majority of patch-clamp studies do observe the appearance of a DIDS-sensitive rectifying Ca^{2+}-sensitive Cl$^-$ conductance that displays little time or voltage dependence under any recording conditions. More recently, the protein product of the vitelliform macular dystrophy (VMD) gene bestrophin encodes a Cl$^-$ channel family that is stimulated by raised intracellular Ca^{2+} (53). The heterologously expressed human bestrophin genes 1 and 2 lead to nonrectifying Cl$^-$ currents that display little time or voltage dependence (53), a feature also observed in recent experiments for both the *X. leavis* bestrophin 2 (24) and mouse bestrophin 2 channels (Hartzel C, personal communication). Thus the properties of the CLCA and VMD conductances bear some resemblance to the CaCCs already described in mammalian epithelial cells (30), including renal collecting duct cells (1, 3, 4, 33, 38). However, whether either of these families underlies the native IMCD CaCC is far from clear, particularly as we do not possess the detailed biophysical or molecular information that is required to answer this important question.

As a first step in answering some of these important issues, our aims were to *1*) determine whether a CaCC is present in native mouse IMCD cells by electrophysiological techniques, *2*) examine in detail the process of CaCC activation by a physiological agonist and the precise relationship between the steady-state biophysical signature of the conductance at different fixed cytosolic Ca^{2+} concentrations,[1] and *3*) determine the single-channel properties of the underlying Ca^{2+}-activated Cl$^-$ channels.

MATERIALS AND METHODS

Cell culture. mIMCD-K2 cells were obtained from Dr. Bruce Stanton (Dartmouth College, Hanover, NH) and grown in Vitrogen 100 (purified collagen)-coated flasks in OptiMem1 with Glutamax-I media supplemented with 10% fetal bovine serum and 50 mg/l penicillin/streptomycin at 37°C in a humidified 5% CO$_2$-95% air atmosphere. Confluent monolayers were subcultured every 7 days by treatment with 0.05% trypsin and 0.2% EDTA in Ca^{2+}- and Mg^{2+}-free PBS. Cells used for patch-clamp measurements and intracellular Ca^{2+} measurements were plated onto 24-mm collagen-coated coverslips at a density of 2×10^4cells/cm^2. Coverslips were then cultured in petri dishes at 37°C in a 5% CO$_2$-95% air atmosphere with medium replacement every 2 days. Experiments were performed in subconfluent cells 2–5 days after seeding.

Isolation of primary mouse IMCD cells. Mice were killed by cervical dislocation. The kidneys were rapidly removed, and cells were selected as described in Kizer et al. (31). The initial one-third of the inner medulla was dissected out and stored for ~10 min in an ice-cold bath solution (patch-clamp bath solution). The tissue was then minced and incubated for 45 min in the bath solution with 0.2% collagenase, 0.2% hyaluronidase, and 0.001% DNAse, kept at 37°C, and continuously gassed with humidified air. Enrichment of IMCD cells was achieved by three centrifugation steps as described in detail by Stokes et al. (52). The density of the final suspension of cell clusters was adjusted to yield subconfluent monolayers, covering approximately one-third of the area of the collagen-coated coverslips on which they were seeded (5). Cells were cultured in mIMCD-K2 media at 37°C in a 5% CO$_2$-95% air atmosphere, with medium replacement every 3 days. Cell cultures were used from *day 4* to *day 7* after preparation. Although the mouse IMCD is composed of two cell types (principle and intercalated cells), the initial part of the IMCD consists primarily (~90%) of principle cells, and thus it is likely that our patch-clamp experiments are derived from these cells. Electrically, we did not observe any differences in the whole cell conductance properties of the cultured cells.

Patch-clamp measurement. Cultured mIMCD cells plated on glass coverslips were transferred to the stage of an inverted microscope for patch-clamp recording. Experiments were performed at room temperature. Pipettes were pulled from borosilicate glass and had resistances, after fire polishing, of 3–6 MΩ. Seal resistances were typically between 5 and 20 GΩ. Whole cell currents were measured with an EPC9 patch-clamp amplifier (HEKA Electronics). Unless otherwise stated, voltage pulses from −80 to +80 mV lasting 1 s with 20-mV increments or voltage ramps from −80 to +80 mV (1-s long) were used to measure membrane currents. The slope conductance was obtained by linear regression of the mean current values at 0.5–1.0 s averaged from voltage steps (held for 1 s) to +80 and −80 mV in 20-mV increments. Reversal potentials (E_{rev}) were determined from voltage ramps from −80 to +80 mV. Voltage stimulation and data acquisition were achieved using 16-bit digital-to-analog and analog-to-digital converters (ITC-16, Instrutech) controlled by a PC using Pulse software (HEKA Electronics). Data were filtered at 1–2 kHz, sampled at 2–5 kHz, and stored on a computer hard disk. Data were analyzed using PulseFit (PulseTools, HEKA Electronics) and SigmaPlot 2001 software (SPSS Science). The fast whole cell as well as the nystatin (100–200 μg/ml) slow whole cell configuration of the patch-clamp technique were used to measure membrane currents (3, 27). Permeability ratios were derived from E_{rev} values using the Hodgkin-Katz modification of the Goldman equation (17). Dose-response curves were fitted to the Hill equation using curve-fitting SigmaPlot 2001 software.

Influence of cation conductance. To reduce the influence of cation conductances on the whole cell current measurements, IMCD cells were cultured in the absence of mineralocorticoids (31) to suppress Na$^+$ (ENaC) expression. Amiloride (10 μM), an inhibitor of ENaC in this cell line (31), had no effect on basal conductance or the CaCC (data not shown, $n = 5$). Furthermore, short-circuit measurements in confluent layers of mIMCD-K2 cells showed only negligible electrogenic Na$^+$ absorption (3). To understand whether any other cationic conductances were present that could influence CaCC measurements all monovalent cations were exchanged in control experiments for *N*-methyl-D-glucamine. This procedure reduced the basal slope conductance to 33 ± 11.1 pS/pF ($n = 9$). This value is significantly different from the slope conductance measured under control conditions ($P < 0.01$; see Fig. 2). But after CaCC activation ($n = 9$) by ionomycin application (200 nM), no significant difference in slope conductance or the size of inward and outward current was observed compared with the standard bath/pipette solution combination. We conclude that cation currents are small compared with the CaCC.

Noise analysis. Nonstationary noise analysis was carried out on fast whole cell currents using a pipette solution containing 0.5 μM intracellular Ca^{2+} concentration ([Ca^{2+}]$_i$) during depolarization-induced activation as well as during hyperpolarization-induced inactivation. Membrane voltages were clamped to −80 mV after maximal Cl$^-$ conductance activation. Current activation was then induced by voltage pulses to +80 or +100 mV for 1-s duration. Thereafter, Cl$^-$ currents were inactivated by membrane hyperpolarization to −80 or −100 mV for 1 s, before the control voltage was restored. This activation-inactivation protocol was repeated 30–50 times in individual cells, and data were filtered at 2 kHz and digitized at 5 kHz. Mean currents were determined for each time point, and the variance was calculated by the method of successive difference (25). Variance data were sampled into 50- or 25-pA bins, so that, for the fitting of the data, equal weights are given to all current levels (25). Single-channel conductance (γ) and number of active channels (*N*) were determined by computer fitting of data to the form

---

[1]During submission of this manuscript, a paper appeared by Qu et al. (44) that described the Ca^{2+} dependency of the mIMCD-K2 CaCC. Results from this paper are very similar to some of the data presented in this study.

$$\sigma^2 = IV\gamma - I^2/N$$

where σ is the current variance, I represents the whole cell current, and V is equal to the command voltage (25). Stationary noise analysis of fast whole cell data was performed by the use of 100- to 200-ms-long current segments recorded every 2 s during conductance inactivation after ATP (100 μM)-induced current activation at a holding potential +60 or +80 mV (3). Analysis was performed as described for nonstationary noise analysis.

Intracellular Ca²⁺ measurement. mIMCD-K2 cells were loaded with 5 μM fura 2 AM by a 35- to 50-min incubation in standard growth media (see *Cell culture*) at 37°C in a 5%CO$_2$-95% air atmosphere. This time period was chosen as it resulted in minimal Ca²⁺ buffering by the indicator but sufficient loading to adequately measure changes in intracellular calcium. The cells were then gently washed three times in the standard bath solution (see below) and fitted into the bath chamber and perfused with this solution (bath volume 0.5 ml, perfusion at 2 ml/min). Cells were imaged using an oil-immersion lens (Fluor 40, N.A.1.3, Nikon). Changes in [Ca²⁺]$_i$ were determined by measuring the fluorescence of fura 2-loaded cells with a dual-wavelength excitation microspectrofluorimeter (Life Science Resources) according to the methods of Grynkiewicz et al. (22). Groups of three to five cells were excited at 340- and 380-nm wavelengths (cycle time 1.2 s) with a xenon-quartz lamp using a Rainbow filter wheel (Life Science Resources) and emitted light filtered using a 510-nm long-pass filter. The emission ratio at the two excitation wavelengths (R) was determined as an index of intracellular Ca²⁺. Background counts were calibrated and automatically subtracted from sampled data. Autofluorescence of unloaded cells was recorded before the commencement of experiments and found to account for 5–8% of the total counts after cell loading only. Absolute [Ca²⁺]$_i$ values were calculated from the fluorescence ratios acquired at 340- and 380-nm excitation wavelengths using the following equation (22)

$$[Ca^{2+}]_i = K_d \times \left(\frac{S_{f2}}{S_{b2}}\right) \times (R - R_{min}) \times (R_{max} - R)$$

where K_d is the dissociation constant of fura 2 for Ca²⁺ (K_d = 224 nM; Ref. 22), S_{f2}/S_{b2} is the fluorescence ratio of the 380 nM signal in the absence of Ca²⁺ to that in the presence of saturating Ca²⁺ (S_{f2}/S_{b2} = 2.6 ± 0.18, n = 8), and R_{min} and R_{max} are the minimal and maximal fluorescence ratios, respectively. R_{min} was obtained by incubating cells in a nominally Ca²⁺- free bath solution containing 5 mM EGTA and 2 μM ionomycin and was 0.48 ± 0.032 (n = 8). R_{max} was obtained by incubating cells in a standard bath solution supplemented with 3 mM CaCl$_2$ (total [Ca²⁺] = 5 mM) and 2 μM ionomycin and was 1.27 ± 0.056 (n = 8).

Rise and decay time measurements. For the Ca²⁺/fura 2 signal (sample rate: 2 Hz), rise times were calculated as follows. The mean basal fluorescence ratio ± SE was calculated. The start of the ATP-dependent Ca²⁺ signal was defined as the last data point before a value higher than the mean basal fluorescence ± SE was reached. Peak fluorescence ratio was achieved when there was no further increase (<1%) between four consecutive data points. The first data point of this series was taken as the peak time. For the current signal, the rise times were determined by two different methods: *1*) continuous current recording (sample rate: 100 Hz) at a fixed holding potential and *2*) voltage ramps between ±80 mV of 1-s duration and a ~1-s interstimulus interval. Times for *method 1* were in principle calculated as described for Ca²⁺/fura 2 signals. The mean basal current ± SE was determined and the start time of the ATP-dependent current signal was defined as the last data point before a value higher than the mean basal current ± SE was reached. Peak was reached when there was no further current increase for 1 s (mean current at 0–0.25 s not significantly different from the mean current at 0.75 to 1 s). The first data point of this series was taken as the peak time. For the decay phase of the Ca²⁺ and the current responses, $t_{1/2}$ values were derived from an exponential fit to the inactivating phase using curve-fitting SigmaPlot software (SigmaPlot 2001, SPSS Science).

Solutions. The standard bath solution used for patch-clamp and fluorescent experiments contained (in mM) 140 NaCl, 4.5 KCl, 1 KH$_2$PO$_4$, 1 MgCl$_2$, 2 CaCl$_2$, 10 HEPES, 6 Tris, and 5 glucose. The pH was adjusted to 7.4 by the addition of Tris. A 10-fold Cl⁻-reduced solution was obtained by replacing 135 NaCl with an isomotically equivalent amount of mannitol. The standard pipette solution contained (in mM) 10 NaCl, 130 KCl, 2 MgCl$_2$, and 10 HEPES. The pH was adjusted to 7.2 by the addition of Tris. In some experiments, all monovalent cations in the bath and pipette solutions were replaced by NMDG⁺. Experiments were conducted under both fast and slow whole cell conditions, and the data were pooled (see Fig. 5), as similar results were obtained under both recording configurations. In some fast whole cell experiments (see Figs. 3, 4, and 6), CaCC was activated directly by perfusion of the cell cytoplasm, via the patch pipette, with solutions of different Ca²⁺ concentrations (0.01–10.0 μM). Appropriate amounts of CaCl$_2$ and EGTA (5 mM) were added to the pipette solution to achieve these free Ca²⁺ concentrations (as calculated using the EQCAL software, Biosoft). Activation of the CaCC was very rapid (<20 s) under these conditions and could not be measured accurately. Note that Ca²⁺ has a finite permeability through the nystatin pore (37), and activation of the CaCC in the slow whole cell configuration was possible, the only difference noted between these fast and slow experiments being that currents took longer to reach steady-state conditions under slow whole cell recordings, but the time course of activation varied with the time to gain good whole cell access. Solutions were adjusted to 320 mosmol/kgH$_2$O by addition of sucrose to avoid activation of swelling-sensitive currents (5).

Materials. Ionomycin (Sigma, Poole, Dorset, UK) was dissolved in ethanol (10⁻² M) and used at 100–200 nM. ATP was made as a stock solution of the Na⁺-salt in the standard bath solution. Fura 2-AM was dissolved in DMSO and obtained from Molecular Probes. Nystatin was from Calbiochem (San Diego, CA). Culture media and all other chemicals were from Sigma.

Statistics. Data are expressed as means ± SE for n separate epithelial cells or groups of three to five cells for fluorescence experiments. Significant difference between mean values was determined using ANOVA with Bonferroni corrections for multiple comparisons applied to Student's *t*-test (unpaired data) for tests between individual data pairs (where appropriate). The level of significance was set at $P \leq 0.05$.

RESULTS

Primary cultures of mouse IMCD contain a Ca²⁺-activated Cl⁻ conductance. Our previous work has shown that the mouse renal IMCD cell line mIMCD-K2 expresses a CaCC that is involved in ATP-stimulated transepithelial Cl⁻ secretion (3). As these cells are an immortalized cell line (31, 32), it was important to establish whether a similar Cl⁻ conductance was present in native mouse IMCD. Figure 1 shows that application of 100 μM ATP to the bathing solution of primary cultures of mouse IMCD cell (see MATERIALS AND METHODS) increased whole cell conductance during slow whole cell patch-clamp recording. Maximal current activation occurred within ~25 s of ATP exposure, but currents then decayed back to basal levels within ~240 s despite the continued presence of ATP (Fig. 1*B*). In four experiments, whole cell conductance increased from 77.2 ± 25.5 to 540.9 ± 58.9 pS/pF. Peak activated currents showed little kinetics (Fig. 1*Ab*) and had an approximately linear *I-V* relationship (Fig. 1*Ad*). Reducing extracellular Cl⁻ concentration 10-fold (mannitol replacement) markedly decreased outward currents and shifted the zero current reversal potential by 39.3 ± 2.4 mV (n = 3), giving a
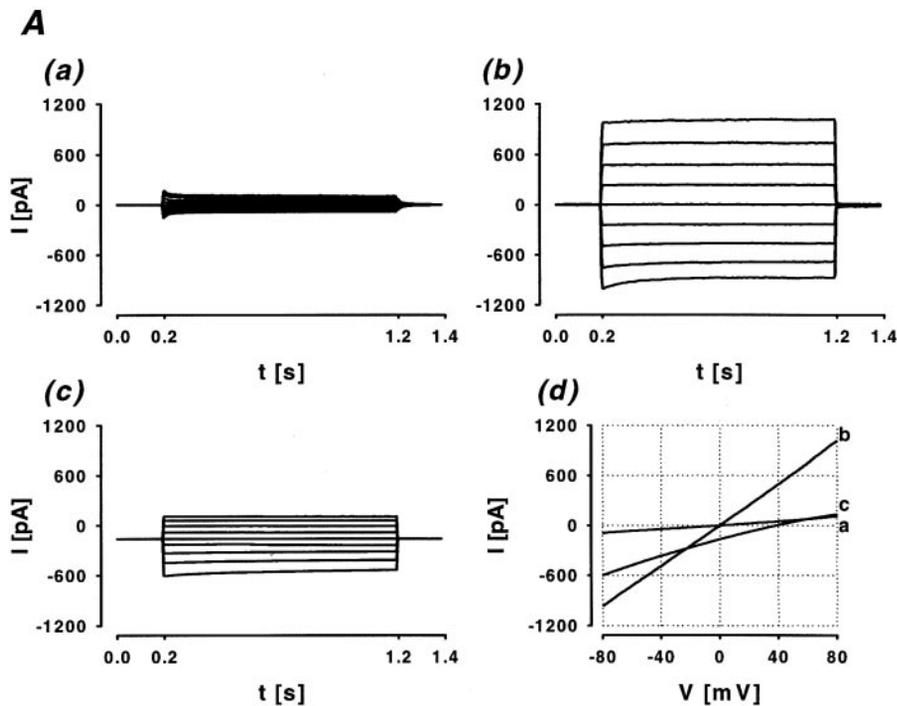
Fig. 1. Activation of a Ca^{2+}-activated Cl^- conductance (CaCC) by ATP in primary cultures of mouse inner medullary collecting duct (IMCD) cells. *A*: examples of whole cell currents, in response to voltage steps from -80 to $+80$ mV in 20-mV increments (*a–c*) and to voltage ramps from -80 to $+80$ mV of 1-s duration (*d*). *a*: Basal response. *b*: Peak ATP response. *c*: Peak ATP response after a 10-fold reduction in bath Cl^-. *d*: Voltage ramps performed under conditions *a–c*. *B*: CaCC slope conductances (conduc.) for control, peak ATP, late ATP (240 s), and in the presence of low-Cl^- (ATP) response. Each bar is the mean of 3–4 cells. Error bars, SE.
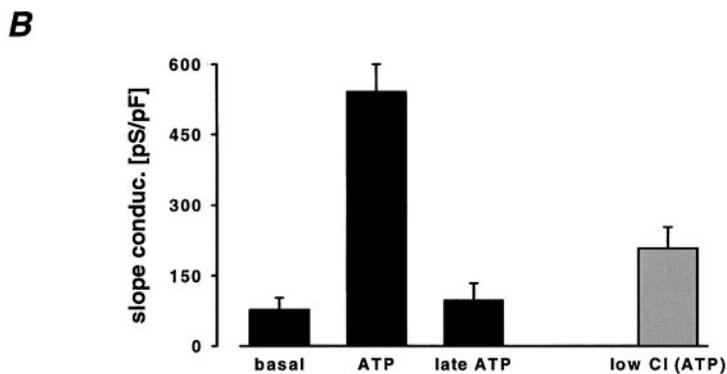
P_{cation}/P_{anion} ratio of 0.1 ± 0.09 (Fig. 1*A*, *c* and *d*), indicating that the ATP-activated currents were predominately anion selective. These results confirm that primary cultures of IMCD cells possess a CaCC with similar biophysical and regulatory properties to the mIMCD-K2 CaCC (3).

Role of cytosolic Ca^{2+} and the activation of the CaCC. Our previous work showed that activation of the CaCC in mIMCD-K2 cells by ATP could be abolished by preloading cells with the Ca^{2+} chelator BAPTA (3). However, we did not assess the relative roles of intra- vs. extracellular Ca^{2+} in the ATP-induced current response. To examine this in more detail, we studied the effect of extracellular Ca^{2+} removal on both the ATP-induced changes in $[Ca^{2+}]_i$ and whole cell Cl^- conductance (Fig. 2, *A* and *B*). In the presence of normal Ca^{2+}, extracellular ATP caused a transient mobilization of $[Ca^{2+}]_i$, which showed a very similar time course to the activation of the CaCC by ATP (Fig. 2, *Aa* and *Ab*, respectively) as we have previously described in these cells (3). In six experiments, the rise time of the $[Ca^{2+}]_i$ signal was 24.9 ± 1.1 s. The decay of the fura signal was well fit to a single exponential with a $t_{1/2}$ of 28.77 ± 4.23 s. The corresponding values for the conductance

changes were 19.4 ± 1.2 and 25.57 ± 2.60 s ($n = 13$), respectively. There is no significant difference between the temporal changes in $[Ca^{2+}]_i$ and the whole cell current response. In these experiments, ATP increased basal whole cell conductance from 117 ± 21.1 to 711 ± 97.3 pS/pF ($n = 13$), values not significantly different from the data for the primary IMCD cell cultures (Fig. 1). In separate experiments, we determined that 100 μM ATP increased $[Ca^{2+}]_i$ from 104 ± 21 nM under resting conditions to peak values of 754 ± 167 nM ($n = 8$) in the presence of 2 mM extracellular Ca^{2+}.

Removal of extracellular Ca^{2+} had no significant effect on either resting $[Ca^{2+}]_i$ or slope conductance (Fig. 2*B*). ATP stimulation of the cells under this condition still resulted in a transient increase in $[Ca^{2+}]_i$ (Fig. 2*Ac*) and associated current response (Fig. 2*Ad*). Although mean peak Ca^{2+}/current values were not different from controls in the absence of extracellular Ca^{2+} (Fig. 2*B*), there was a significant reduction in the decay time of both signals ($t_{1/2}$ of Ca^{2+} signal $= 22.39 \pm 4.24$ s, and for the current response the decay time was 21.14 ± 2.64 s, $P < 0.01$ vs. respective controls). This latter result suggests that part of the activation of the CaCC, during the late phase of
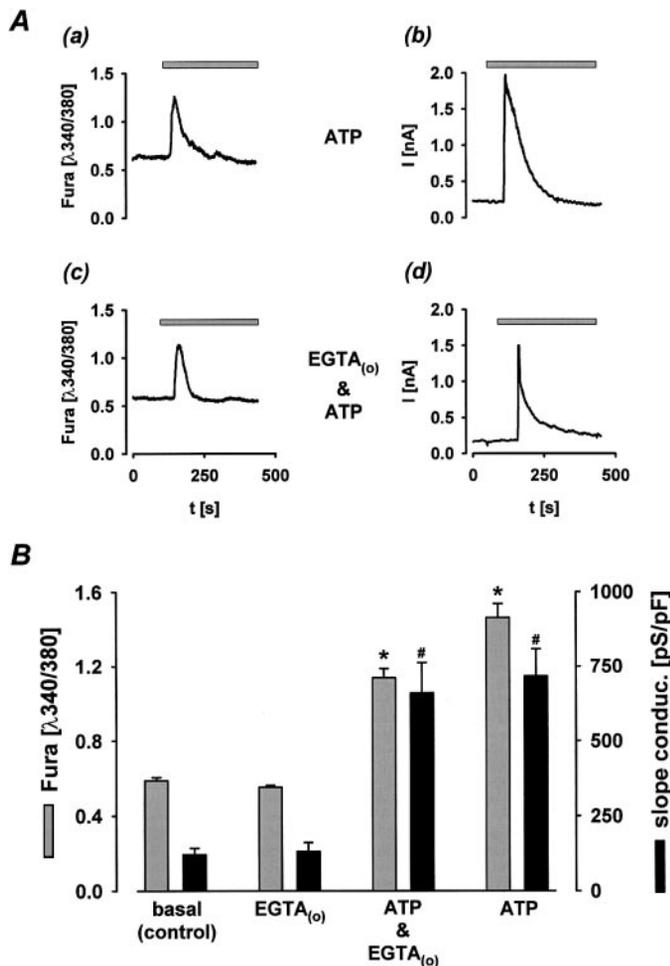
Fig. 2. Intracellular Ca^{2+} release is responsible for activation of the CaCC by extracellular ATP in mIMCD-K2 cells. *A*: examples of typical fura 2 (*a* and *c*) and current (*b* and *d*) responses (nystatin slow whole cell configuration, holding potential +80 mV) under different experimental conditions. Bar indicates 100 μM ATP application. EGTA was present during the whole experiment. *B*: peak fura 2 response and peak CaCC slope conductance. Each bar is the mean of between 3 and 13 experiments. Error bars, SE; basal, control conditions; EGTA$_{(o)}$, no extracellular Ca^{2+} present; ATP, bath application of 100 μM ATP. * and #: Significantly different ($P < 0.001$) from basal (control).

the ATP response, is due to Ca^{2+} influx across the plasma membrane.

Properties of the CaCC of mIMCD-K2 cells at different levels of [Ca^{2+}]$_i$. As ATP only produced a transient increase in the CaCC, intracellular Ca^{2+} perfusion was used to investigate the steady-state properties of the CaCC. Under control conditions, mIMCD-K2 cells displayed a small membrane conductance of 101.0 ± 21.1 pS/pF (Fig. 3*A*). At a [Ca^{2+}]$_i$ of 10 nM, no evidence for the CaCC was obtained, even at large positive voltages (Fig. 3*Aa*). This demonstrates that the underlying Ca^{2+}-activated Cl^- channels have an absolute requirement for intracellular Ca^{2+} to open. At a [Ca^{2+}]$_i$ of 100 nM, whole cell currents were also very small, but in a proportion of cells (6/13) slow outward current relaxations were observed in response to the largest positive voltage jumps; in the other cells, only leakage currents were obtained. Increasing [Ca^{2+}]$_i$ to 500 nM increased whole cell conductance, and current relaxations of large amplitude were obtained (Fig. 3*Ba*). Under these conditions, outward currents consisted of two compo-

nents: a small instantaneous time-independent component and a larger, slowly activating time- and voltage-dependent component. After activation at depolarizing potentials, clear tail currents on hyperpolarization were characteristically observed. Inward currents were small in comparison but significantly different from basal values. A comparison of instantaneous with steady-state current levels taken at the time points indicated showed a clear difference, illustrating the time-dependent activation of the channels at depolarizing potentials (Fig. 3*Bb*). Increasing [Ca^{2+}]$_i$ to 1.0 μM and above, whole cell conductance was further increased, but the relaxations were of small amplitude or not present at all, indicating that the channels were (nearly) fully activated at all potentials tested (Fig. 3, *Ca* and *Da*). Associated *I-V* curves (instantaneous and steady-state) were essentially the same (Fig. 3, *Cb* and *Db*). Figure 4 summarizes the Ca^{2+} dependence of the CaCC plotted in the form of a dose-response curve at two holding potentials (−80 and +80 mV). The data were well fitted to the Hill equation (see MATERIALS AND METHODS) and gave EC$_{50}$ values of 650.5 ± 31.4 nM at −80 mV and 306.1 ± 44.6 nM at +80 mV ($P < 0.05$). The associated Hill coefficients were 3.0 ± 0.3 and 1.7 ± 0.4 ($P < 0.05$), respectively.

Steady-state kinetics of the Ca^{2+}-activated Cl^- currents. Relaxations of Ca^{2+}-activated Cl^- currents were most prominent at a [Ca^{2+}]$_i$ of 0.5 μM. This section first describes these relaxations and then compares the results with those obtained at other [Ca^{2+}]$_i$. Figure 5, *A* and *B*, shows activation and deactivation current relaxations obtained at [Ca^{2+}]$_i$ of 0.5 μM. All relaxations, both activation at positive voltages (Fig. 5*A*) and deactivation at negative voltages (Fig. 5*B*), could be satisfactorily fitted with single exponentials. Currents displayed voltage- and time-dependent activation at positive potentials with an "on" time constant (τ) of 303 ± 31 ms at 20 mV that decreased to 220 ± 31.4 ms at 80 mV ($P < 0.05$, Fig. 5*C*). Marked current deactivation was also observed at negative potentials, although this showed little dependence on holding potential and had "off" time constants in the region of 100–160 ms over the potential range 0 to −80 mV (Fig. 5*C*). The simplest interpretation of these relaxations is that they reflect a two-state kinetic scheme

$$C \rightleftharpoons O$$

where C and O are the closed and open states of the channel, respectively. Instantaneous current ratios (instantaneous current at holding potential/test potential) were identical at the onset and the end of pulses. This does not rule out an additional, very fast kinetic process, but it does suggest that such a process, if present, does not affect the voltage dependence of the open-closed scheme. Furthermore, there was no evidence of a slower kinetic process. Even for very long lasting (≥ 2 s) voltage steps, current responses were very steady once the relaxations were completed. Tail current amplitudes and kinetics were not affected by pulse duration. Such effects are found in sensory neurons (39), for example. Mean values of τ measured at a [Ca^{2+}]$_i$ of 1 μM are shown as a function of voltage in Fig. 5*C*. At test voltages of −80 to 0 mV, the off time constants are not significantly different from those measured at an [Ca^{2+}]$_i$ of 0.5 μM, but the on time constants, measured between +20 and +80 mV are significantly smaller, indicating that increasing cytosolic Ca^{2+} speeds channel opening but does not affect the closing process. Although τ values
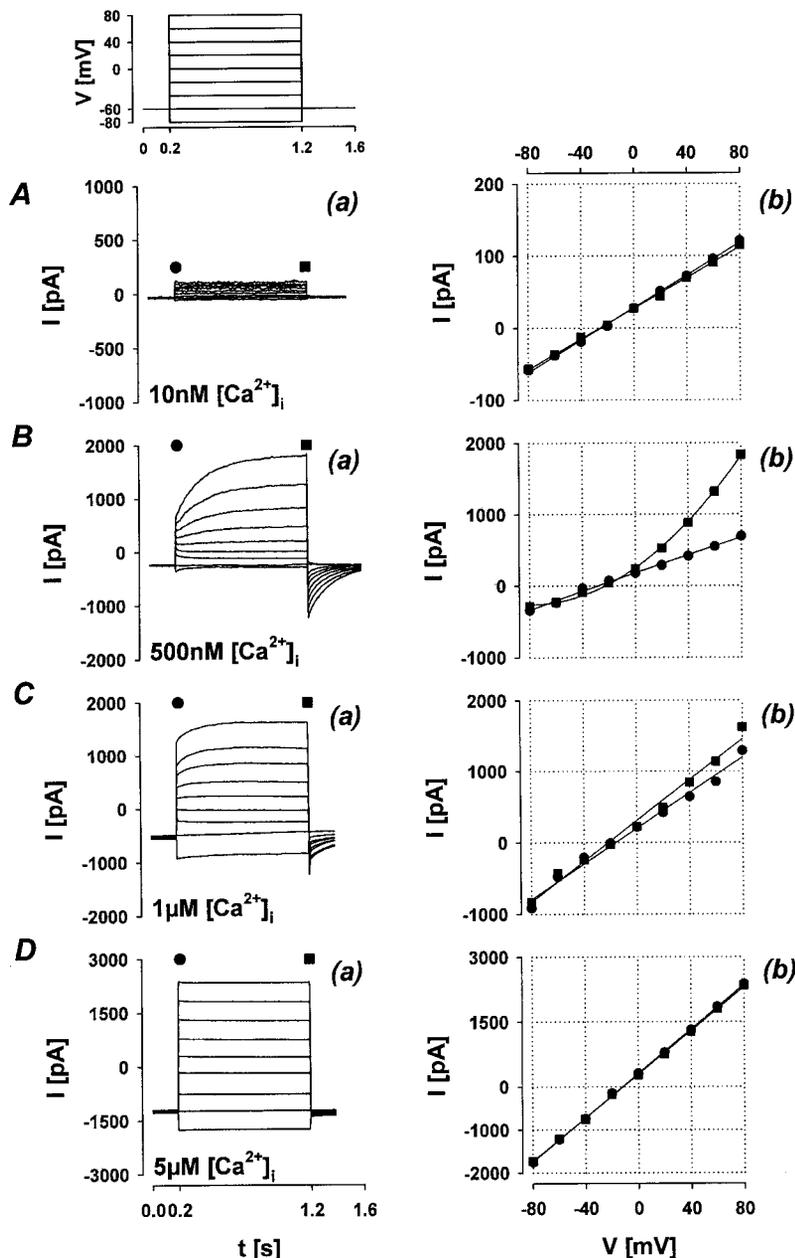
Fig. 3. Effect of increasing intracellular Ca^{2+} concentration ($[Ca^{2+}]_i$) on the biophysical characteristics of the CaCC in mIMCD-K2 cells. *a*: Whole cell current (fast whole cell configuration) responses to voltage steps from -80 to 80 mV in 20-mV steps (*inset*). *b*: Associated current-voltage (*I-V*) relationships for instantaneous (●) and steady-state (■) currents (see MATERIALS AND METHODS) after the voltage steps. $[Ca^{2+}]_i$.= 10 nM (*A*), 500 nM (*B*); 1 μM (*C*), and 5 μM (*D*).

were not obtained systematically at other $[Ca^{2+}]_i$, the general trend was a reduction in the on time constants with increasing $[Ca^{2+}]_i$ at positive test potentials.

Single-channel properties: noise analysis. In cell-attached experiments, application of ionomycin or ATP to mIMCD-K2 cells led to an overall increase in current noise, but we were not able to clearly resolve single-channel events ($n = 32$, data not shown). To obtain an estimate of unitary conductance, we employed a population-based measurement of single-channel conductance and density by performing stationary (Fig. 6*A*) and nonstationary noise analysis (Fig. 6*B*) on whole cell currents (see MATERIALS AND METHODS). Stationary noise analysis yielded a single-channel conductance of 6.2 ± 0.8 pS and a channel density per cell of $5,561 \pm 311$ ($n = 5$). Nonstationary noise analysis generated a single-channel conductance of 7.1 ± 0.9 pS and a density of $4,251 \pm 251$ ($n = 6$), values not significantly different to the stationary values.

DISCUSSION

We have shown that extracellular ATP activates a CaCC in primary cultures of mouse IMCD cells. To our knowledge this is the first demonstration that native mouse IMCD cells possess a chloride conductance that is regulated by changes in intracellular calcium. The native mouse IMCD conductance displayed similar biophysical properties to the CaCC in the mIMCD-K2 cell line (3). The fact that extracellular ATP (3, 4, 36) and kinins (33) stimulate transepithelial Cl⁻ secretion in these mIMCD-K2 cells, suggests that Ca^{2+}-dependent Cl⁻ channels are involved in anion secretion in the native mouse IMCD. Clearly direct secretory studies on isolated IMCDs are now required to confirm this hypothesis.

Regulation of the CaCC by Ca^{2+}. In the presence of normal extracellular $[Ca^{2+}]$, 100 μM ATP caused a transient increase in both $[Ca^{2+}]_i$ and the CaCC. Both parameters exhibited
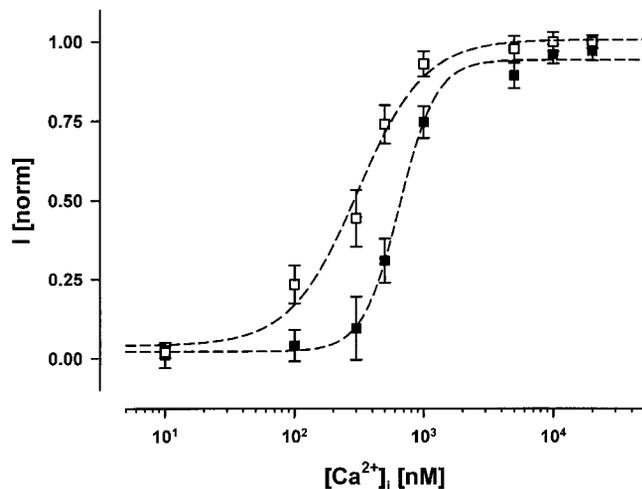
Fig. 4. $[Ca^{2+}]_i$ dose-response curve of the CaCC in mIMCD-K2 cells. Dependence of the steady-state Ca^{2+}-activated Cl^- currents (fast whole cell configuration) measured at $+80$ (□) and -80 mV (■) on $[Ca^{2+}]_i$. CaCC conductance was normalized to the maximal current achieved ($+80$ mV $= 1,685 \pm 135$ pA; $-80 = 1,634 \pm 122$ pA). Each point is the mean of between 4 and 10 cells. Error bars, SE. Data were fit to the Hill equation (see MATERIALS AND METHODS).

similar rise times to peak and decay times to baseline levels. Because the shape and time course of transepithelial inward secretory short-circuit current in ATP-stimulated mIMCD-K2 epithelial layers are also very similar to the changes in $[Ca^{2+}]_i$ and the CaCC (3), these results suggest that a strong coupling exists between changes in cytosolic Ca^{2+} and Cl^- secretion. Removing extracellular Ca^{2+} had very little effect on either the time course or magnitude of the change in $[Ca^{2+}]_i$ or the maximal ATP-induced Cl^- conductance. Thus an increase in $[Ca^{2+}]_i$, caused by activation of G protein-coupled purinoceptors and Ca^{2+} release from intracellular stores is sufficient and directly activates the CaCC on the apical membrane of mIMCD-K2 cells. These results are consistent with previous molecular and functional data that identified P2Y$_1$ and P2Y$_2$ purinergic receptors in these cells (36). Removal of extracellular Ca^{2+} did, however, speed up the decay time of the whole cell current, indicating that normally the influx of Ca^{2+} plays some role in the activation of the CaCC. This Ca^{2+} could enter through P2X receptors (36) and/or store-operated channels. Taken together, these results suggest that no additional regulatory step, such as channel phosphorylation, is required for activation of the IMCD CaCC, although, without further experiments, we cannot at this stage discount a role for regulation by other proteins. A similar tight coupling between $[Ca^{2+}]_i$ and channel activity has been observed for the Ca^{2+}-activated Cl^- channel of *X. laevis* oocyte membranes (6, 34) and mouse parotid and pancreatic acinar cells (15). In contrast, Ca^{2+}-activated channels in some human epithelial cells, including pancreatic duct, biliary duct, and intestinal epithelial cell lines (18, 26, 48, 60, and reviewed in Ref. 30), are dependent on both an increase in $[Ca^{2+}]_i$ and activation of calmodulin kinase II. Similarly, the bovine CLCA channel is also modulated by calmodulin kinase II, whereby phosphorylation results in an increase in the sensitivity of the channel to cytosolic Ca^{2+} (13). Whether calmodulin is involved in modulating the effects of Ca^{2+} on the mIMCD K2 CaCC is presently unknown.

Kinetics of the CaCC and implications for Cl^- transport in IMCD cells. The whole current data in Figs. 3–5 show that the activation of the CaCC is very sensitive to cytosolic Ca^{2+} over the normal physiological range. At 0.5 μM $[Ca^{2+}]_i$, all cells studied displayed currents that slowly activated at positive potentials and deactivated quickly at negative potentials. Kinetic analysis revealed that activation time constants varied with holding potential, whereas inactivation constants were not appreciably voltage-dependent and that the decline in whole cell current was due to a voltage-dependent decrease in the sensitivity of the channels to Ca^{2+}. Similar results have been reported for the CaCC in lacrimal acinar cells (10, 35). Thus at this level of $[Ca^{2+}]_i$, activation of the IMCD CaCC would not lead to substantial inward current flow because of the inherent inactivation of the channels at negative membrane potentials. In contrast, increasing $[Ca^{2+}]_i$ to ~1 μM or above led to large, nonrectifying whole cell currents at all potentials, indicating that the channels under these conditions were nearly fully activated even at physiological membrane potentials. Therefore, at this level of $[Ca^{2+}]_i$, the CaCC would provide a large inward (secretory) current. From the Hill plots (Fig. 4), the binding of Ca^{2+} to the channel is seen to be a cooperative process, and one dependent on membrane potential. Similar results have been observed for the CaCC of pancreatic acinar cells (10), endothelial cells (42), and oocytes (34).

Comparison of the properties of the native CaCC to expressed mCLCA and bestrophins. Cunningham et al. (8) cloned the first gene (bCLCA1) resembling bovine tracheal CaCC (45) and demonstrated that transfection of bCLCA1 into COS-7 cells induced an ionomycin-activated, nonrectifying Cl^- conductance. These bCLCA1 currents showed no kinetics and were blocked by the reducing agent DTT but not niflumic acid. In contrast, expression of bCLCA1 in *X. laevis* oocytes produced an outwardly rectifying current in the absence of any Ca^{2+} ionophore compared with antisense or water-injected oocytes. Similar to the bCLCA1-induced currents in COS-7 cells, the oocyte conductance was inhibited by DTT and DIDS and was insensitive to niflumic acid (8). More recent studies on other isoforms have also produced conflicting results. In HEK cells transfected with mouse CLCA1 (14), human CLCA1 (19), or human CLCA2 (21), Ca^{2+}-dependent Cl^- currents could be evoked by inclusion of either a very high concentration (2 mM) of Ca^{2+} in the patch pipette or by exposure to ionomycin. These Ca^{2+}-activated Cl^- currents were outwardly rectifying and displayed no kinetics at any membrane voltages. All the expressed currents were shown to be sensitive to inhibition by DTT and DIDS but significantly were also blocked by niflumic acid. In *X. laevis* oocytes, mCACC/mCLCA1 expression was associated with a spontaneous elevation of an outwardly rectifying, time-independent Cl^- current that was also blocked by DIDS (47), similar to that observed for bCLCA1 expressed in oocytes (8). In contrast to mouse or human CLCA1 or 2, Elble et al. (9) recently showed that mCLCA4 expression in HEK-293 cells induced an ionomycin- and methacholine-activated nonrectifying whole cell current but which still displayed no time or voltage-dependent gating. The data in Fig. 3 indicate that outwardly rectifying currents could be observed at cytosolic Ca^{2+} concentrations up to ~500 nM. However, these currents always displayed marked activation/deactivation relaxations that contributed to the rectification of the conductance. As cytosolic Ca^{2+} was
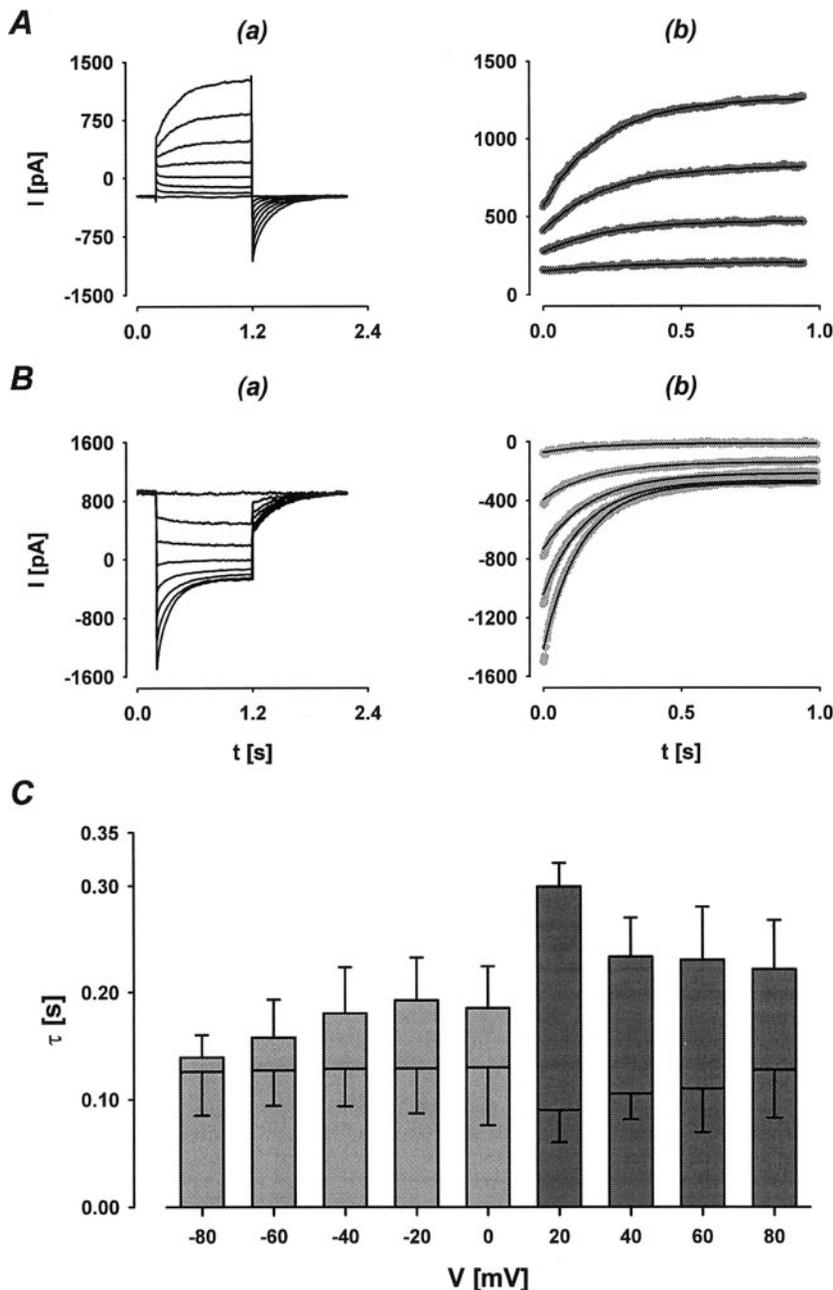
Fig. 5. Characteristics of the Ca^{2+}-activated Cl$^-$ currents in mIMCD-K2 cells. Kinetics of relaxations. *Aa*: family of currents (fast whole cell configuration) evoked using a pipette solution containing 500 nM Ca^{2+} at voltages between -60 and $+80$ mV in 20-mV increments, with an interpulse interval of 5 s. Holding potential = -60 mV. *Ab*: plot of "on"-relaxation in *Aa*. Superimposed lines show the exponential fits for the outward current relaxations at 20, 40, 60, and 80 mV. *Ba*: family of currents (fast whole cell configuration) evoked using a pipette solution containing 500 nM Ca^{2+} at voltages between -80 and $+60$mV in 20-mV increments, with an interpulse interval of 5 s. Holding potential = $+60$ mV. *Bb*: plot of "off"-relaxation in *Ba*. Superimposed lines show the exponential fits for the inward current relaxations at -20, -40, -60, and -80 mV. *C*: plot of on and off time constants (τ) as a function of membrane potential. Values (SE) for 500 nM (*top* error bars) and 1 μM (*bottom* error bars) are shown. Each point is the mean of between 4 and 7 cells with currents pooled from both nystatin slow and fast whole cell configurations.

increased, the kinetics were lost, and current rectification disappeared, indicating that the underlying channels display no intrinsic Cl$^-$ current rectification. Therefore, over a range of fixed Ca^{2+} concentrations (0.01–10 μM), we were unable to reproduce the whole cell data for mCLCA1 (14). However, our results are similar to the properties of mCLCA4 (9), at least after maximal stimulation.

Less information is available about the single-channel properties of CLCA members. Unitary conductance for bCLCA1 and hCLCA1 are in the region of 15–30 pS (8, 19). Our noise analysis studies yielded a unitary conductance of ~6 pS, which suggests that CLCAs are unlikely to encode the native IMCD CaCC (but see discussion on multiple expression below). Single-channel studies from other cells suggest that a variety of different Ca^{2+}-activated Cl$^-$ channels exists (30). Unitary

conductances range from 1–3 pS in oocytes, acinar cells, and different types of muscle cells, up to 30 pS in bovine tracheal cells (30). In addition, the ORCC channel, in which some groups have observed modulation by cytosolic Ca^{2+} in excised inside-out patches, has a conductance of between 50 and 70 pS (11). Thus the IMCD channel appears more related to the oocyte and acinar Ca^{2+}-activated channels, both at the single-channel and whole cell level.

Because multiple CLCA gene expression is seen in IMCD cells (3, 33), it is possible that unique subunit structures may confer appropriate tissue-specific properties on mammalian CaCCs. Clearly, coexpression studies are now required to test this possibility. In this context it is interesting that the properties of the endogenous CaCC from another IMCD-derived cell line, mIMCD-3 (4), are very similar to those of mCLCA1, as
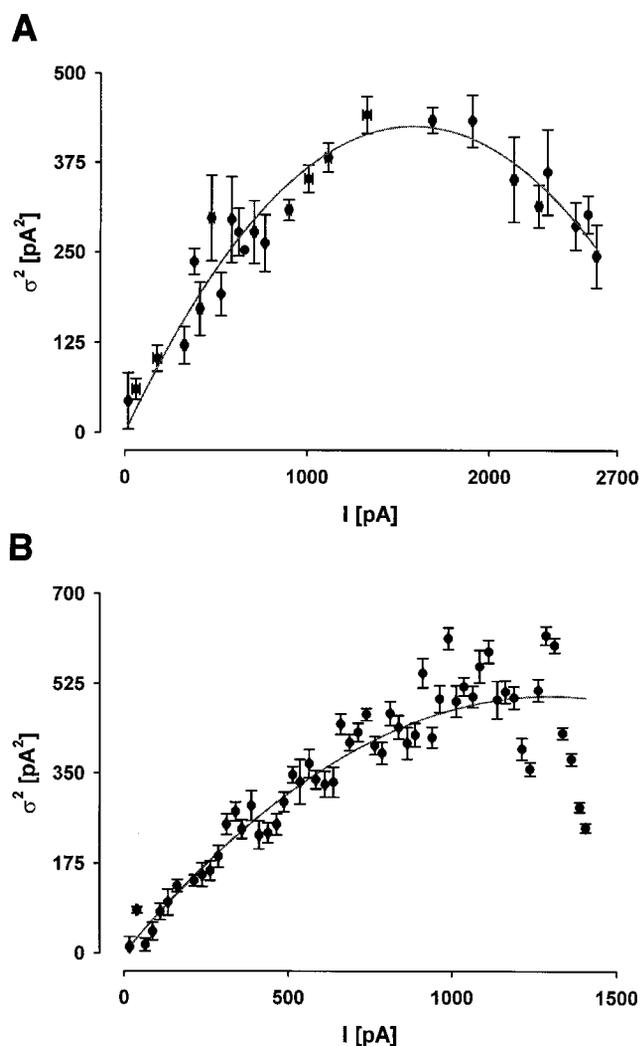
A

B

Fig. 6. Noise analysis of whole cell Ca²⁺-activated Cl⁻ currents in mIMCD-K2 cells. Whole cell current stationary ($n = 5$; *A*) and nonstationary ($n = 6$; *B*) noise analysis (see MATERIALS AND METHODS for further details) is shown. σ, Current variance.

well as hCLCA1 and 2, expressed in HEK cells. We have previously shown that mIMCD-3 cells also express multiple CLCA transcripts (4). Until coexpression and/or knockout studies have been performed with all CLCA isoforms in an appropriate cell system, we cannot be certain about the exact relationship between multiple CLCA expression and the electrophysiological data.

Transient transfection of human type 1 and 2 bestrophin cDNAs in HEK cells (53) produced nonrectifying, time- and voltage-independent whole currents that were reversibly inhibited by the disulfonic stilbene DIDS. In transfected cells, Cl⁻-selective currents were found to be spontaneously active, but further increases in conductance were observed on raising intracellular Ca²⁺ (53). Thus the basic properties of the bestrophin-induced conductance do bear some important similarities to the fully activated IMCD CaCC, as well as to bCLCA1 and mCLCA4. However, further work on the Ca²⁺ sensitivity of the bestrophin-induced currents, and importantly the expression of bestrophins in mouse renal cells, is required before a critical comparison can be made.

Is there a physiological role of the CaCC in the IMCD? Models of renal function with details at the cellular level have been developed for most nephron segments, including the IMCD (see Ref. 62 for references). However, as recently acknowledged by Weinstein (62), considerable uncertainty remains about important transport events. One such uncertainty is the role of apical Cl⁻ channels in collecting duct function. Physiological studies in isolated tubules often monitor the basal situation and rarely investigate acute regulation by luminal and/or peritubular stimuli. Recent work makes it clear that cAMP-regulated fluid secretion does occur along the collecting duct (16, 61), and our results extend this to suggest that intracellular Ca²⁺ probably does as well. Therefore, the current models of tubular function need to be refined to incorporate these additional transport events at the apical membrane.

From electrophysiological studies of CFTR (3, 17, 56), cAMP activates a nonrectifying, anion-selective conductance that displays little time and voltage dependence. Hence the biophysical properties of the channel can readily explain how an increase in cAMP stimulates an inward (secretory) current under conditions where intracellular Cl⁻ (anions) is accumulated above electrochemical equilibrium and at physiological membrane potentials. In the case of the IMCD CaCC, the situation is more complicated. Our kinetic and dose-response analysis of the whole cell currents clearly shows that below 100 nM the channels are inactive and therefore cannot contribute to basal Cl⁻/fluid secretion. The conductance only become active when $[Ca^{2+}]_i$ is raised above a certain threshold value (~300–500 nM.). However, even at these levels of Ca²⁺, there is minimal inward (secretory) current because of the intrinsic gating (inactivation) of the channels at negative membrane potentials (Figs. 3 and 5). It should be noted that at these submaximal Ca²⁺ levels, if the membrane potential were depolarized, for example, due to the increase in current flow across the apical membrane, the Cl⁻ permeability through the CaCC would be further enhanced due to the voltage-dependent change in sensitivity of the channels to cytosolic Ca²⁺.

Raising $[Ca^{2+}]_i$ to values greater than ~700 nM, however, leads to the activation of conductance with kinetic properties very similar to CFTR, and under these conditions the CaCC would readily provide a robust inward current at all potentials. However, in contrast to cAMP activation of CFTR, stimulation of the CaCC by nucleotides and kinins is transient (3, 33, and the current study), and therefore this Ca²⁺-stimulated pathway is unlikely to have a major role in sustained transepithelial Cl⁻ secretion from the IMCD. By analogy, with the surface epithelium of the airways (54) the renal CaCC may be more important in fine-tuning the net agonist-stimulated secretion from the IMCD, in response to local agonists such as mucosal nucleotides. Net secretion would be further enhanced by mucosal ATP via an inhibition of amiloride-sensitive Na⁺ channels, as described by McCoy et al. (36), in mIMCD-K2 layers. Recent measurements of bulk ATP concentration in rat proximal tubular fluid were in the region of ~250 nM (58). Because renal epithelial cells possess very active surface ectonucleotidases, the local concentration of ATP is certainly much higher (58). If a similar situation existed in the IMCD, then our results would predict that luminal ATP would cause near maximal rises in $[Ca^{2+}]_i$ and thus a large inward current due to activation of the CaCC (assuming a membrane potential of about −40 to −60 mV) (3). Physiologically, such a process would

provide regulation of NaCl loss to urine. Importantly, coexpression of CFTR with CaCC at the apical plasma membrane would allow multiple natriuretic stimuli to act synergistically via the rate-limiting Cl⁻ exit step (64) to promote net anion secretion over net Na⁺ absorption.

Pathophysiological role of CaCC. Fluid accumulation in renal cystic disease is likely to be dependent on the same cellular process as described above. Because it has been shown that only ~50% of autosomal dominant polycystic kidney disease (ADPKD) cysts express CFTR (23), it seems likely that other anion channels, such as the CaCC, may be important as the anion exit pathway in the remaining cystic structures. Wilson et al. (63) showed that ATP was released into the lumen of cysts derived from primary cultures of renal epithelia cells from polycystic kidneys and later showed that cystic cells secrete enhanced amounts of ATP compared with normal (non-PKD) cells (50). This autocrine mechanism is likely to lead to CaCC activation and stimulation of fluid secretion. Indeed, extracellular nucleotide signaling is a common feature along the entire nephron, including the IMCD (49). In principle cells isolated from bpk ARPKD mice, Cl⁻ secretion is stimulated by increases in intracellular cAMP and Ca²⁺, strongly suggesting the participation of an apical CaCC (57).

Recent work in primary cilia has also provided a possible link to PKD (41). Primary cilia are found in renal epithelial cells and have been shown to be involved in transducing changes in fluid flow into an increase in intracellular Ca²⁺ (43). Polycystin 1 and 2 are located at the cilium, whereas polycystin 1 ablation abolishes the ability of the cilium to sense flow (41). Ultimately, activation of apical Cl⁻ channels (CaCCs or CFTR), must underlie fluid secretion and fluid accumulation within cysts. Clearly, a detailed analysis of CaCC regulation in health and disease states is now indicated.

REFERENCES

1. **Bidet M, Tauc M, Rubera I, De Renzis G, Poujeol C, Bohn MT, and Poujeol P.** Calcium-activated chloride currents in primary cultures of rabbit distal convoluted tubule. *Am J Physiol Renal Fluid Electrolyte Physiol* 271: F940–F950, 1996.
2. **Boese SH, Aziz O, Gray MA, and Simmons NL.** Intracellular Ca²⁺ directly regulates the Ca²⁺-activated Cl⁻ conductance in mouse inner medullary collecting duct cells (Abstract). *J Gen Physiol* 122: 87, 2003.
3. **Boese SH, Glanville M, Aziz O, Gray MA, and Simmons NL.** Ca²⁺ and cAMP-activated Cl⁻ conductances mediate Cl⁻ secretion in a mouse renal inner medullary collecting duct cell line. *J Physiol* 523: 325–338, 2000.
4. **Boese SH, Sayer J, Stewart G, Glanville M, Gray MA, and Simmons NL.** Renal expression of Ca²⁺-activated Cl⁻ channels. *Curr Top Membr Transpl* 53: 283–307, 2002.
5. **Boese SH, Wehner F, and Kinne RKH.** Taurine permeation through swelling-activated anion conductance in rat IMCD cells in primary culture. *Am J Physiol Renal Fluid Electrolyte Physiol* 271: F498–F507, 1996.
6. **Callamaras N and Parker I.** Ca²⁺-dependent activation of Cl⁻ currents in *Xenopus* oocytes is modulated by voltage. *Am J Physiol Cell Physiol* 278: C667–C675, 2000.
7. **Ciampolillo F, McCoy DE, Green RB, Karlson KH, Dagenais A, Molday RS, and Stanton BA.** Cell specific expression of amiloride-sensitive, Na⁺-conducting ion channels in the kidney. *Am J Physiol Cell Physiol* 271: C1303–C1315, 1996.
8. **Cunningham SA, Awayda MS, Bubien JK, Ismailov II, Arrate MP, Berdiev BK, Benos DJ, and Fuller CM.** Cloning of an epithelial channel from bovine trachea. *J Biol Chem* 270: 31016–31026, 1995.
9. **Elble RC, Ji G, Nehrke K, DiBiasio J, Kingsley PD, Kotlikoff MI, and Pauli BU.** Molecular and functional characterization of a murine calcium-activated chloride channel expressed in smooth muscle. *J Biol Chem* 277: 18586–18591, 2002.
10. **Evans MG and Marty A.** Calcium-dependent chloride currents in isolated cells from rat lacrimal glands. *J Physiol* 378: 437–460, 1986.
11. **Frizzell RA, Rechkemmer G, and Shoemaker RL.** Altered regulation of airway epithelial cell chloride channels in cystic fibrosis. *Science* 33: 558–560, 1986.
12. **Fuller CM and Benos DJ.** Electrophysiology of the CLCA family. *Curr Top Membr Transpl* 53: 389–414, 2002.
13. **Fuller CM, Ismailov II, Keeton DA, and Benos DJ.** Phosphorylation and activation of a bovine tracheal anion channel by Ca²⁺/calmodulin-dependent protein kinase II. *J Biol Chem* 269: 26642–26650, 1994.
14. **Gandhi R, Elble RC, Gruber AD, Schreur KD, Ji HL, Fuller CM, and Pauli BU.** Molecular and functional characterization of a calcium-sensitive chloride channel from mouse lung. *J Biol Chem* 273: 32096–32101, 1998.
15. **Giovannucci DR, Bruce JIE, Straub SV, Arreola J, Sneyd J, Shuttleworth TJ, and Yule DI.** Cytosolic Ca²⁺ and Ca²⁺-activated Cl⁻ current dynamics: insights from two functionally distinct mouse exocrine cells. *J Physiol* 540.2: 469–484, 2002.
16. **Grantham JJ and Wallace DP.** Return of the secretory kidney. *Am J Physiol Renal Physiol* 282: F1–F9, 2002.
17. **Gray MA, Pollard CE, Harris A, Coleman L, Greenwell JR, and Argent BE.** Anion selectivity and block of the small conductance chloride channel on pancreatic duct cells. *Am J Physiol Cell Physiol* 259: C752–C761, 1990.
18. **Gray MA, Winpenny JP, Verdon P, O'Reilly CM, and Argent BE.** Properties and role of calcium-activated chloride channels in pancreatic duct cells. *Curr Top Membr Transpl* 53: 231–256, 2002.
19. **Gruber AD, Elble RC, Ji HL, Schreur KD, Fuller CM, and Pauli BU.** Genomic cloning, molecular characterization, and functional analysis of human CLCA1, the first human member of the family of Ca²⁺-activated Cl⁻ channel proteins. *Genomics* 54: 200–214, 1998.
20. **Gruber AD, Elble RC, and Pauli BU.** Discovery and cloning of the CLCA gene family. *Curr Top Membr Transpl* 53: 368–387, 2002.
21. **Gruber AD, Schreur KD, Ji HL, Fuller CM, and Pauli BU.** Cloning, transmembrane structure and function of CLCA2 a Ca²⁺-activated Cl⁻ channel from human lung, trachea and mammary gland. *Am J Physiol Cell Physiol* 276: C1261–C1270, 1999.
22. **Grynkiewicz G, Poenie M, and Tsein RY.** A new generation of Ca²⁺ indicators with greatly improved fluorescence properties. *J Biol Chem* 260: 3440–3450, 1985.
23. **Hanaoka K, Devuyst O, Schwiebert EM, Wilson PD, and Guggino WD.** A role for CFTR in human autosomal polycystic kidney disease. *Am J Physiol Cell Physiol* 270: C389–C399, 1996.
24. **Hartzell HC, Qu ZQ, Wei R, Mann W, and Fischmeister R.** Molecular physiology of calcium-activated chloride channels. *J Gen Physiol* 122: 22, 2003.
25. **Heinemann SH and Conti F.** Non-stationary noise analysis and application to patch-clamp recordings. *Methods Enzymol* 207: 131–148, 1992.
26. **Ho MWY, Kaetzel MA, Armstrong DL, and Shears SB.** Regulation of a human chloride channel. *J Biol Chem* 276: 18673–18680, 2001.
27. **Horn R and Marty A.** Muscarinic activation of ionic currents measured by a new whole-cell recording method. *J Gen Physiol* 92: 145–159, 1988.
28. **Husted RF and Stokes JB.** Separate regulation of Na⁺ and anion transport by IMCD: location, aldosterone, hypertonicity, TGF-β₁ and cAMP. *Am J Physiol Renal Fluid Electrolyte Physiol* 271: F433–F439, 1996.
29. **Husted RF, Zhang C, and Stokes JB.** Concerted actions of IL-1β inhibit Na⁺ absorption and stimulate anion secretion by IMCD cells. *Am J Physiol Renal Physiol* 275: F946–F954, 1998.
30. **Kidd JF and Thorn P.** Intracellular Ca²⁺ and Cl⁻ channel activation in secretory cells. *Annu Rev Physiol* 62: 493–513, 2000.
31. **Kizer NL, Lewis B, and Stanton BA.** Electrogenic sodium absorption and chloride secretion by an inner medullary collecting duct cell line

(mIMCD-K2). *Am J Physiol Renal Fluid Electrolyte Physiol* 268: F347–F355, 1995.

32. **Kizer NL, Vandorpe D, Lewis B, Bunting B, Russell J, and Stanton BA.** Vasopressin and cAMP stimulate electrogenic chloride secretion in an IMCD cell line. *Am J Physiol Renal Fluid Electrolyte Physiol* 268: F854–F861, 1995.

33. **Kose H, Boese SH, Glanville M, Gray MA, Brown CDA, and Simmons NL.** Bradykinin regulation of salt transport across mouse inner medullary duct epithelium involves activation of a Ca^{2+}-dependent Cl^- conductance. *Br J Pharmacol* 131: 1689–1699, 2000.

34. **Kuruma A and Hartzell HC.** Bimodal control of a Ca^{2+}-activated Cl^- channel by different Ca^{2+} signals. *J Gen Physiol* 115: 59–80, 1999.

35. **Marty A, Tan YP, and Trautmann A.** Three types of calcium-dependent channel in rat lacrimal glands. *J Physiol* 357: 293–325, 1984.

36. **McCoy DE, Taylor AL, Kudlow BA, Karlson KE, Slattery MJ, Schwiebert LM, Schwiebert EM, and Stanton BA.** Nucleotides regulate NaCl transport across mIMCD-K2 cells via P2X and P2Y purinergic receptors. *Am J Physiol Renal Physiol* 277: F552–F559, 1999.

37. **McNamara B, Winter DC, Cuffe JE, O'Sullovan GC, and Harvey BJ.** Basolateral K^+ channel involvement in forskolin-activated chloride secrertion in human colon. *J Physiol* 519: 251–260, 1999.

38. **Meyer K and Korbmacher C.** Cell swelling activates ATP-dependent voltage gated chloride channels in M1 mouse cortical collecting duct cells. *J Gen Physiol* 108: 177–193, 1996.

39. **Meyer ML.** A calcium-activated chloride current generates the after depolarization of rat sensory neurons in culture. *J Physiol* 364: 217–239, 1985.

40. **Morales MM, Carrol TP, Morita T, Schwiebert EM, Devuyst O, Wilson PD, Lopes AG, Stanton BA, Dietz HC, Cutting GR, and Guggino WB.** Both the wild-type and a functional isoform of CFTR are expressed in kidney. *Am J Physiol Renal Fluid Electrolyte Physiol* 270: F1038–F1048, 1996.

41. **Nauli SM, Alenghat FJ, Luo Y, Williams E, Vassilev P, Li X, Elia AEH, Lu W, Brown EM, Quinn SJ, Ingber DE, and Zhou J.** Polycystins 1 and 2 mediate mechanosensation in the primary cilium of kidney cells. *Nature Gen* 33: 129–137, 2003.

42. **Nilius B, Prenen J, Szucs G, Wei L, Tanzi F, Voets T, and Droogmans G.** Calcium-activated chloride channels in bovine pulmonary artery endothelial cells. *J Physiol* 498: 381–396, 1997.

43. **Praetorius HA and Spring KR.** Bending the MDCK primary cilium increases intracellular calcium. *J Membr Biol* 184:71–79, 2001.

44. **Qu Z, Wei RW, and Hartzell HC.** Characterization of Ca^{2+}-activated Cl^- currents in mouse kidney inner medullary collecting duct cells. *Am J Physiol Renal Physiol* 285: F326–F335, 2003.

45. **Ran S, Fuller CM, Arrate MP, Latorre R, and Benos DJ.** Functional reconstitution of a chloride channel protein from bovine trachea. *J Biol Chem* 267: 20630–20637, 1992.

46. **Rauchman MI, Nigam SK, Delpire E, and Gullans SR.** An osmotically tolerant inner medullary collecting duct cell line from an SV40 transgenic mouse. *Am J Physiol Renal Fluid Electrolyte Physiol* 265: F416–F424, 1993.

47. **Romio L, Musante L, Cinti R, Seri M, Moran O, Zegarra-Moran O, and Galietta LJV.** Characterisation of a murine gene homologous to the bovine CaCC chloride channel. *Gene* 228: 181–188, 1999.

48. **Schlenker T and Fitz JG.** Ca^{2+}-activated Cl^- channels in a human biliary cell line: regulation by Ca^{2+}/calmodulin-dependent protein kinase. *Am J Physiol Gastrointest Liver Physiol* 271: G304–G310, 1996.

49. **Schwiebert EM and Kishore BK.** Extracellular nucleotide signalling along the renal epithelium. *Am J Physiol Renal Physiol* 280: F945–F963, 2001.

50. **Schwiebert EM, Wallace DP, Braunstein GM, King SR, Peti-Peterdi J, Hanaoka K, Guggino WB, Guay-Woodford LM, Bell PD, Sullivan LP, Grantham JJ, and Taylor AL.** Autocrine extracellular purinergic signaling in epithelial cells derived from polycystic kidneys. *Am J Physiol Renal Physiol* 282: F763–F775, 2002.

51. **Simmons NL.** Renal epithelial Cl^- secretion. *Exp Physiol* 78: 117–137, 1993.

52. **Stokes JB, Grupp C, and Kinne RKH.** Purification of rat papillary collecting duct cells: functional and metabolic assessment. *Am J Physiol Renal Fluid Electrolyte Physiol* 253: F251–F262, 1987.

53. **Sun H, Tsunenari T, King-Wai Y, and Nathan J.** The vitelliform macular dystrophy protein defines a new family of chloride channels. *Proc Natl Acad Sci USA* 99: 4008–4013, 2002.

54. **Tarran RT, Loewen ME, Paradiso AM, Olsen JC, Gray MA, Argent BE, Boucher RC, and Gabriel SE.** Regulation of murine airway surface liquid volume by CFTR and Ca^{2+}-activated Cl^- conductances. *J Gen Physiol* 120: 407–418, 2002.

55. **Vandorpe DH, Ciampolillo F, Green RB, and Stanton BA.** Cyclic nucleotide-gated cation channels mediate sodium absorption by IMCD (mIMCD-K2) cells. *Am J Physiol Cell Physiol* 272: C901–C910, 1997.

56. **Vandorpe DH, Kizer N, Ciampollilo F, Moyer B, Karlson K, Guggino WG, and Stanton BA.** CFTR mediates electrogenic secretion in mouse inner medulla collecting duct (mIMCD-K2) cells. *Am J Physiol Cell Physiol* 269: C683–C689, 1995.

57. **Veizis EI, Carlin CR, and Cotton CU.** Decreased amiloride-sensitive Na^+ absorption in collecting duct principle cells isolated from BPK ARPKD mice. *Am J Physiol Renal Physiol* 286: F244–F254, 2004.

58. **Vekaria RM, Unwin RJ, and Shirley DG.** Endogenous ATP concentrations in proximal convoluted tubules of the rat (Abstract). *J Physiol* 552: 62P, 2003.

59. **Volk KA, Sigmund RD, Snyder PM, McDonald FJ, Welsh MJ, and Stokes JB.** rENaC is the predominant Na^+ channel in the apical membrane of the rat renal inner medullary collecting duct. *J Clin Invest* 96: 2748–2757, 1995.

60. **Wagner JA, Cozen AL, Schulman H, Gruenert DG, Stryer L, and Gardner P.** Activation of chloride channels in normal and cystic fibrosis airway epithelial cells by multifunctional calcium/calmodulin-dependent protein kinase. *Nature* 349: 793–796, 1991.

61. **Wallace DP, Rome LA, Sullivan LP, and Grantham JJ.** cAMP-dependent fluid secretion in rat inner medullary collecting ducts. *Am J Physiol Renal Physiol* 280: F1019–F1029, 2001.

62. **Weinstein AM.** Mathematical models of renal fluid and electrolyte transport: acknowledging our uncertainty. *Am J Physiol Renal Physiol* 284: F871–F884, 2003.

63. **Wilson PD, Hovater JS, Casey CC, Fortenberry JA, and Schwiebert EM.** ATP release mechanisms in primary cultures of epithelia derived from the cysts of polycystic kidneys. *J Am Soc Nephrol* 10: 218–229, 1999.

64. **Zeidel ML.** Hormonal regulation of inner medullary collecting duct sodium transport. *Am J Physiol Renal Fluid Electrolyte Physiol* 265: F159–F173, 1993.

65. **Zhang C, Husted RF, and Stokes JB.** Effect of cAMP agonists on cell pH and anion transport by cultured rat inner medullary collecting duct cells. *Am J Physiol Renal Fluid Electrolyte Physiol* 270: F131–F140, 1996.